Cryst. Res. Technol.	37	2002	4	391–406

U. KAISER*, J. BISKUPEK, D. A. MULLER[1], K. GÄRTNER, CH. SCHUBERT

Institut für Festkörperphysik, Friedrich-Schiller Universität, Jena 07743, Germany
[1]Bell Laboratories, Lucent Technologies, Murray Hill, NJ 07974, USA

Properties of GeSi Nanocrystals Embedded in Hexagonal SiC

In this paper high-resolution electron microscopy investigations and molecular dynamics simulations of GeSi nanocrystals buried in *4H*-SiC are performed, showing that the experimentally observed shapes of the GeSi nanocrystals are strongly correlated with their orientational relationships. Measurements of the lattice spacing suggest that the nanocrystals are strained. Quantum confinement in selected nanocrystals has been detected using spatially-resolved electron energy loss spectroscopy performed in conjunction with atomic resolution annular dark-field scanning TEM.

Keywords: HRTEM, implantation, Ge-Nanocrystals, Molecular dynamics, EELS-HAADF, Quantum confinement

(Received February 28, 2002; Accepted March 7, 2002)

Introduction

Modern device features are rapidly approaching the atomic scale [MULLER (a)] and the behaviour of solids in the nanometer size regime became one of the most active areas in materials research. It has been demonstrated experimentally that nanosized Ge crystals buried in SiO_2 show a quantum size effect and efficient optical transitions, when they are smaller than 5 nm [TAKEOKA] although the size dependence of the photon energy is much weaker than calculated [NIQUET]. For small Ge and Si nanocrystals buried in hexagonal SiC, calculations predict quantum confinement [WEISSKER] and direct optical transitions [KATULA] as well, however experimental confirmation has not been presented so far. Further, not only may the size of the nanocrystals have an important impact on the electronical properties, but also their structure, shape [DAHMEN], and orientation within the crystalline matrix. The great lattice mismatch between Ge and SiC (about 27% in [110] projection) is expected to result in differently strained interfaces for different orientations of the nanocrystal with respect to the matrix. For Si/GaAs and Si/Ge systems it has already been demonstrated experimentally that different interface strains (which originates from different orientation-relationships between matrix and layer) produces different electronic properties [PERESSI (a), COLOMBO]. Further, first principle calculation of unstrained InP/GaInAs hetero-structures showed no difference in the electronic properties for different orientation-relationships [PERESSI (b)].

Z-contrast dark-field imaging in a scanning TEM (STEM) [CREWE] or in the conventional TEM [THON, KAISER (a)] is suitable for determining the size distribution of buried nanocrystals if the difference in atomic number (Z) from the matrix is large. Since the

* corresponding author: kaiser@pinet.uni-jena.de

© WILEY-VCH Verlag Berlin GmbH, 13086 Berlin, 2002 0232-1300/02/0404-0391 $ 17.50+.50/0

high angle scattering signal from a single atom is strongly dependent on the atomic number (roughly $Z^{1.7}$) [LOANE, HOWIE, PENNYCOOK], atomic-scale imaging in annular dark-field (ADF)-STEM can also be used to determine the chemical content of a nanocrystal, if the contributing elements are known, and the sample is thin. ADF-imaging can be performed simultaneously with the analysis of the inelastically scattered electrons collected by an on-axis electron energy-loss spectrometer (EELS), allowing atomic-scale spectroscopy [BATSON (a), BROWNING, MULLER (a) & (b)] and the direct correlation between image and spectrum. High-resolution transmission electron microscopy (HRTEM) is able to reveal the lattice, size, shape, and orientation-relationship to the matrix of a particular nanocrystal. HRTEM studies of GeSi nanocrystals created by ion implantation in *4H* and *6H*-SiC [SCHUBERT] have recently been reported [KAISER (b)] and the content of selected crystals has been determined to be about 80% Ge and 20% Si. However, no detailed investigations about shapes, size distributions and preferred orientations of the embedded nanocrystals have been presented so far. As GeSi nanocrystals within SiC comprise a highly lattice-mismatched system, reordering of the atoms at the interface due to strain relaxation will take place. If the chemical content of the GeSi nanocrystals is known, its lattice strain can be determined from lattice fringe spacing measurements and the achievable accuracy for the case of nanosized clusters in a crystalline matrix has been determined to be about 0.001-0.05 Å, depending on the order of reflections which can be measured [DE RUIJTER, CROZIER].

For the theoretical investigation of the reordering of a strained interface there exist in principle three methods: classical molecular dynamics (MD) computer simulation, finite element simulation and quantum mechanical first principle calculations. The method of finite elements [CHRISTIANSEN, BENABBAS] does not provide atomic-level information and the first principle methods [KOHN] are up to now restricted to systems with a maximum number of about 10^3 atoms [WEISSKER]. Classical MD is the appropriate method as it can be used to simulate atomic processes in systems with a large number of atoms up to 10^6 within a time scale up to nanoseconds. The reliability of MD simulations depends strongly on the quality of the potential used. Most common potentials are the Tersoff-potential [TERSOFF (a), (b) & (c)] and the Stillinger-Weber-potential [STILLINGER]. The Tersoff-potential has especially been prepared and tested for the simulation of systems containing group IV elements. It has already been demonstrated that using this potential, structural properties calculated for graphite, diamond, amorphous C, crystalline Si and Ge agree reasonable well with the experimental data [MORIGUCHI, TERSOFF (d)]. Moreover, the structures of cage clusters of group IV elements and their properties calculated using the Tersoff-potential match sufficiently well the first principle calculations [MORIGUCHI]. In addition, the Tersoff-potential has been proved to be relevant for determining the stability and growth of Ge-particles inside an amorphous Ge matrix [BORDING].

When using the relaxed atomic coordinates from MD calculations for the simulation of HRTEM-images, direct comparison with experiment is possible. A few combined studies have already been reported in the literature for nanocrystals in or on top of a crystalline matrix [SCHEERSCHMIDT, PAUWELS (a) & (b), WERNER]. Moreover, MD simulations have been successfully applied to determine energetically preferred nanocrystal orientation-relationships [ZIMMERMANN, LANÇON] and the dependence of the particle stability on its shape and orientation has been studied using Monte-Carlo simulations [COMBE]. However, to the best of our knowledge, no reports on combined MD and HRTEM studies for group IV materials have been presented so far.

In this paper we study by classical MD-simulations, why buried GeSi nanocrystals of particular shape exist in particular orientations only. We apply high spatial resolution EELS simultaneously with atomic resolution HAADF-STEM to small nanocrystals to receive experimental confirmation on quantum confinement.

Experimental

Cross-sectional samples for TEM examination were prepared from high dose ($1x10^{16}$ cm^{-2}), high temperature (700°C) 250 keV Ge and 110 keV Si ion implanted hexagonal SiC after annealing at 1600°C for 120 sec. (For more details about the implantation process see [SCHUBERT]). Mechanical polishing, dimpling and low-angle Ar-ion milling were used. Conventional and high-resolution TEM was carried out using a JEOL 3010 TEM equipped with a LaB_6 cathode and atomic-resolution high-angle annular dark-field scanning TEM (ADF-STEM) was carried out in a FEG-JEOL2010 equipped with an electron energy loss spectrometer (EELS). HRTEM image simulations on the base of the relaxed atom coordinates from molecular dynamics calculation have been performed using the programs MacTempas [O'KEEFE] and Dial-Multislice [CHUVILIN] based on the multislice method [COWLEY].

Model preparation for molecular dynamics calculations

Molecular dynamics calculations have been performed with a standard MD code [GÄRTNER] using the Tersoff potential [TERSOFF (c)]. The initial system of the nanocrystal embedded in the crystalline *4H*-SiC matrix (MD cell) has been prepared in the following way.

First, spherical and facetted Ge nanocrystals with average diameters of about 5 nm to 6 nm (about 3000 to 5000 Ge atoms) were built. The structure used is the diamond structure of the unstrained bulk Ge at T = 0 K. However regular stacking faults were introduced because the HRTEM images showed that the nanocrystals have a high degree of hexagonality [KAISER (b)]. The facets of the nanocrystals are $\{0001\}$, $\{1\bar{1}01\}$, $\{1\bar{1}00\}$ and $\{11\bar{2}0\}$ planes in accordance with the hexagonal crystal symmetry. For a special orientation of a Ge nanocrystal with respect to the *4H*-SiC matrix the relation between the facets of the nanocrystal (shown in [0001] projection) and that of the matrix (shown in $[11\bar{2}0]$ projection) is given in Fig. 1a in accordance with the HRTEM view depicted in Fig. 1b. As can be seen, the facets of the hexagonal Ge nanocrystal shown in Fig. 1b correspond qualitative well with those formed in the case of macroscopic hexagonal SiC crystals, shown in Fig. 1c (both are close to a [0001] near projection). Because the experimental investigations showed that the nanocrystals do not only consist of Ge but also contain Si, nanocrystals were allowed to be of mixed composition. This was taken into account for selected cases by replacing randomly chosen Ge atoms by Si atoms and changing the lattice parameter according to the Vegard's law.

Second, the prepared nanocrystal was embedded in an ideal *4H*-SiC crystal fixed in $[11\bar{2}0]$ projection with a size up to $9\times9\times9$ nm^3 (MD cell about 70,000 atoms). The embedding is performed by removing all Si and C atoms of the SiC matrix with a distance to any of the nanocrystal atoms smaller than a critical one. The critical distances are chosen to be 2.4 Å for Si in accordance to the Si-Ge bond length and 2.5 Å for C, which is larger than

the C-Ge bond length (2.0 Å). This enlargement is reasonable as more Si-Ge than C-Ge bonds are expected at the interface because no stable phase of GeC exists [PANDEY]. The nanocrystal is embedded with different orientations and different positions around the matrix centre. The position for each orientation is varied in all three directions in a range of -1 Å to 1 Å (steps of 0.1 Å) around the centre of the *4H*-SiC crystal.

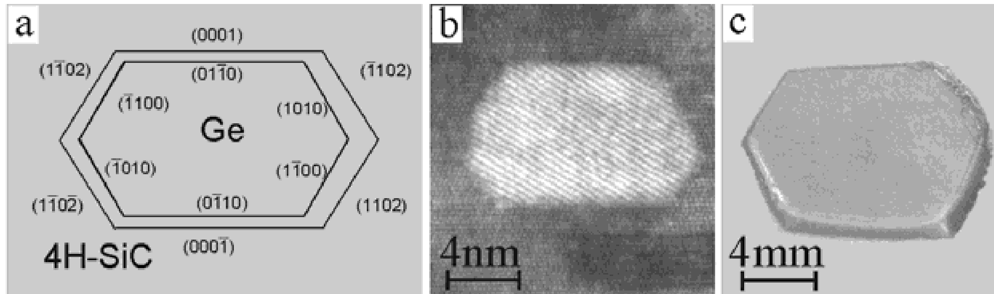

Fig. 1: (a) Scheme of facets of GeSi dots within hexagonal SiC, (b) atomic resolution ADF-STEM image of a GeSi nanocrystal inside *4H*-SiC and (c) optical micrograph of hexagonal SiC. (Note the different scale of the images.)

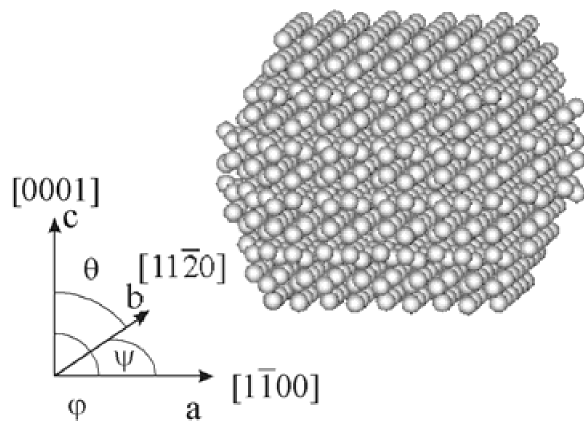

Fig. 2: Model of a nanocrystal together with the corresponding directions a, b, c and angles ϑ, φ, ψ used. (ϑ is the angle around the a-axis, φ is the angle around the b-axis, ψ is the angle around the c-axis).

The orientation is described by three rotation angles ϑ, φ, ψ for rotation around the axes a, b, c, respectively, as seen in Fig. 2. The angles were varied between 0° to 180° (in 0.5° to 10° steps). For each orientation and position the potential energy of the whole system was calculated (about 2,000,000 calculations) with periodic boundary conditions and a canonical ensemble (constant number of atoms, constant volume and constant temperature). For each orientation, the position with the lowest potential energy was determined and then for this configuration a fast static zero temperature relaxation has been performed until the minimum of the total potential energy is reached with an accuracy of 0.1 eV. For selected cases in addition dynamical relaxations have been performed at high temperatures using the velocity form of the Verlet-algorithm [VERLET]. However, with respect to the stability, these calculations did not show significant changes.

Result and discussion

Fig. 3 shows a high-angle centered dark-field image where the GeSi nanocrystals are revealed by their Z-contrast [KAISER (a)]. The corresponding size distribution of the nanocrystals is given in Fig. 4. As can be seen, many nanocrystals are about 5 nm in size. The orientation-relationships between the nanocrystals and the *4H*-SiC matrix in [11$\bar{2}$0] projection can be divided into four main view types. It was found that all different nanocrystal projections are only different views of hexagonal GeSi nanocrystals, [KAISER (b)].

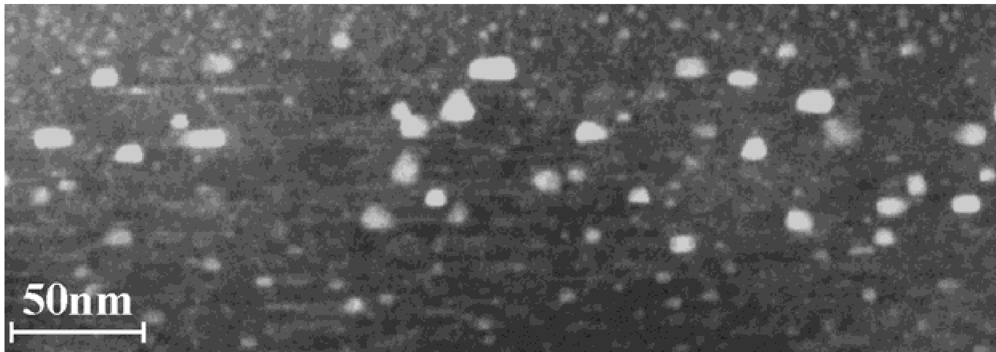

Fig. 3: High-angle centered dark-field image showing the distribution of GeSi nanocrystals buried in SiC, which are visible because of the atomic-number difference between nanocrystal and matrix elements.

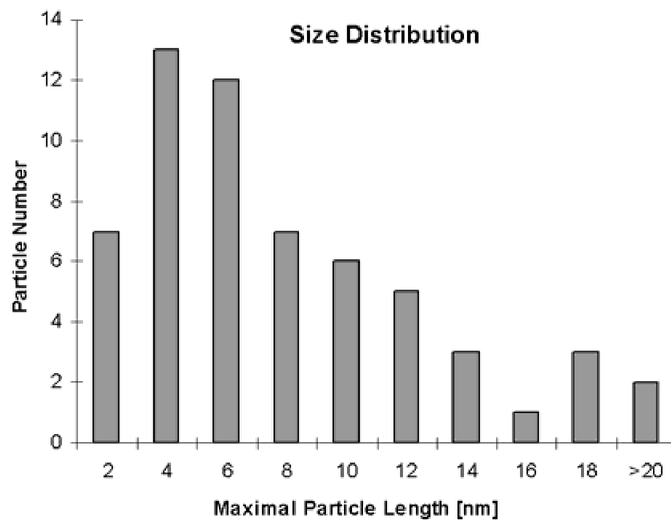

Fig. 4: Size distribution corresponding to Fig. 3 showing that many nanocrystals are already smaller than 5nm in size.

In Fig. 5 examples of nanocrystals viewed in [11$\bar{2}$0] *4H*-SiC matrix projection are seen. In Fig. 6 the corresponding diffractograms are presented. Each row shows nanocrystal (NC) examples of the same view group. The orientation-relationships between nanocrystal and matrix in the four view-groups called A, B, C, and D are:

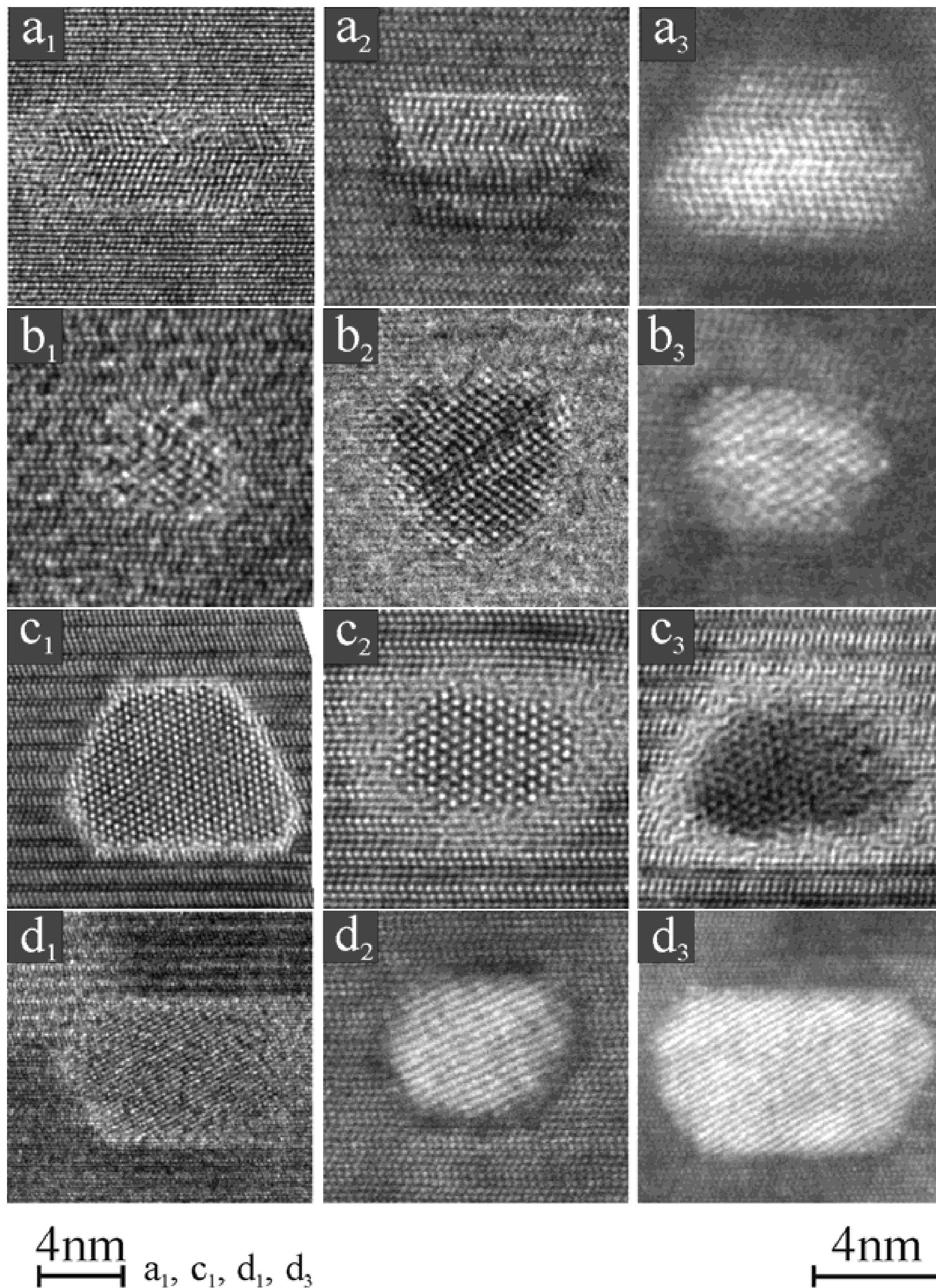

Fig. 5: $11\bar{2}0$ HRTEM- and atomic resolution HAADF-STEM images of GeSi nanocrystals in the four main views found: (a_1-a_3): $[0001]_{NC}$ parallel $[0001]_{4H\text{-SiC}}$, $[11\bar{2}0]_{NC}$ parallel $[11\bar{2}0]_{4H\text{-SiC}}$ (view A), (b_1-b_3): $[11\bar{2}0]_{NC}$ parallel $[11\bar{2}0]_{4H\text{-SiC}}$, ($c_1$-$c_3$): $[0001]_{NC}$ perpendicular $[0001]_{4H\text{-SiC}}$, d_1-d_3: the NC shows mainly only one $\{01\bar{1}0\}$ lattice plane. (The scale marker on the left refers to Figs a_1, c_1, d_1, d_3, that on the right to all other images.)

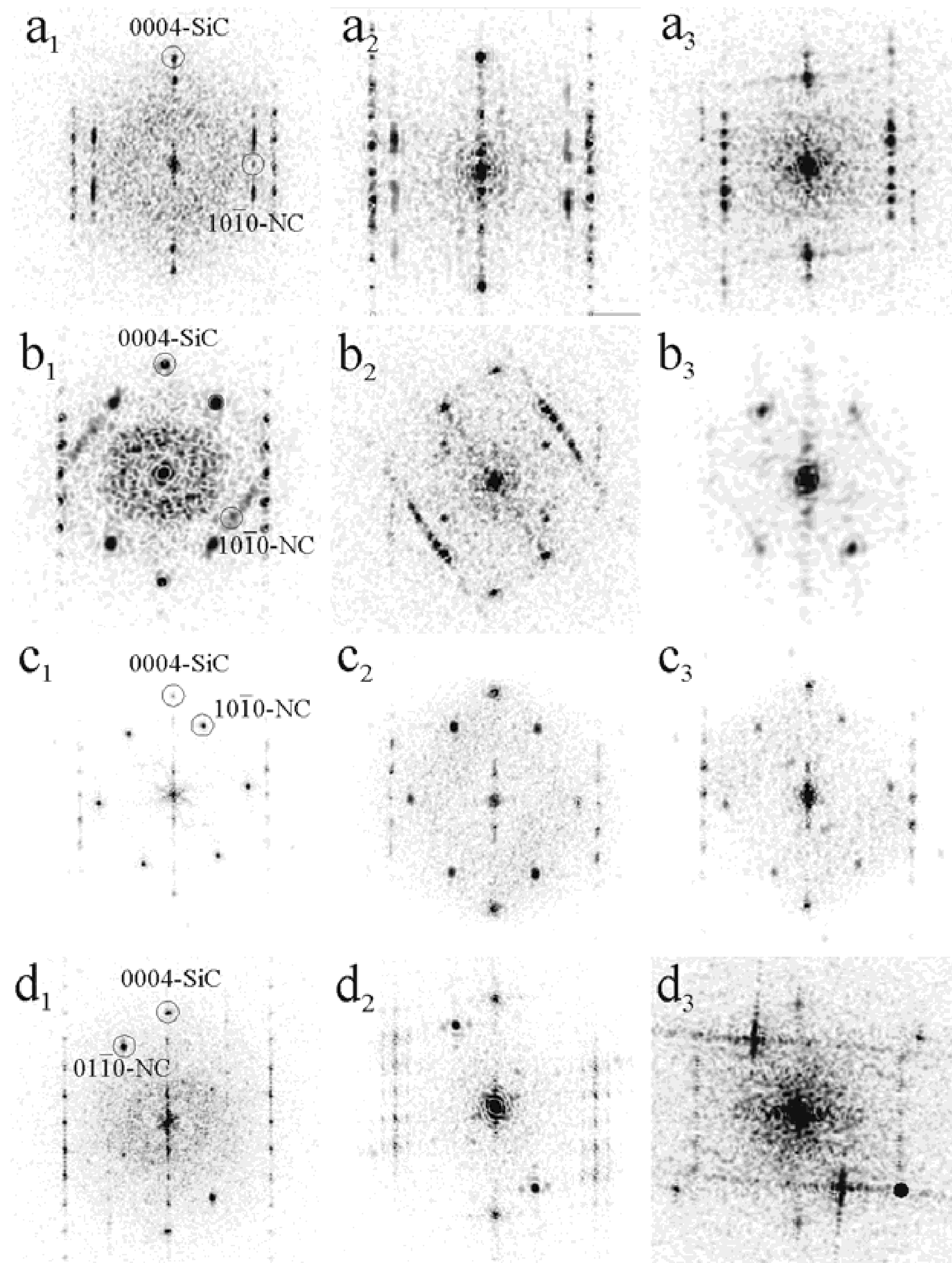

Fig. 6: Diffractograms corresponding to the nanocrystals in Fig. 5.

A $[0001]_{NC}$ parallel $[0001]_{4H\text{-SiC}}$, $[11\bar{2}0]_{NC}$ parallel $[11\bar{2}0]_{4H\text{-SiC}}$, (Figs 5,6 a_1-a_3)

B $[11\bar{2}0]_{NC}$ parallel $[11\bar{2}0]_{4H\text{-SiC}}$ or $[11\bar{2}0]_{NC}$ inclined to $[11\bar{2}0]_{4H\text{-SiC}}$, (Figs 5,6 b_1-b_3)

C $[0001]_{NC}$ perpendicular $[0001]_{4H\text{-SiC}}$, (Figs 5,6 c_1-c_3)

D $[0001]_{NC}$ inclined to $[0001]_{4H\text{-SiC}}$ and to $[01\bar{1}0]_{4H\text{-SiC}}$, showing one set of $\{01\bar{1}0\}$ lattice plane fringes only, (Figs 5,6 d_1-d_3).

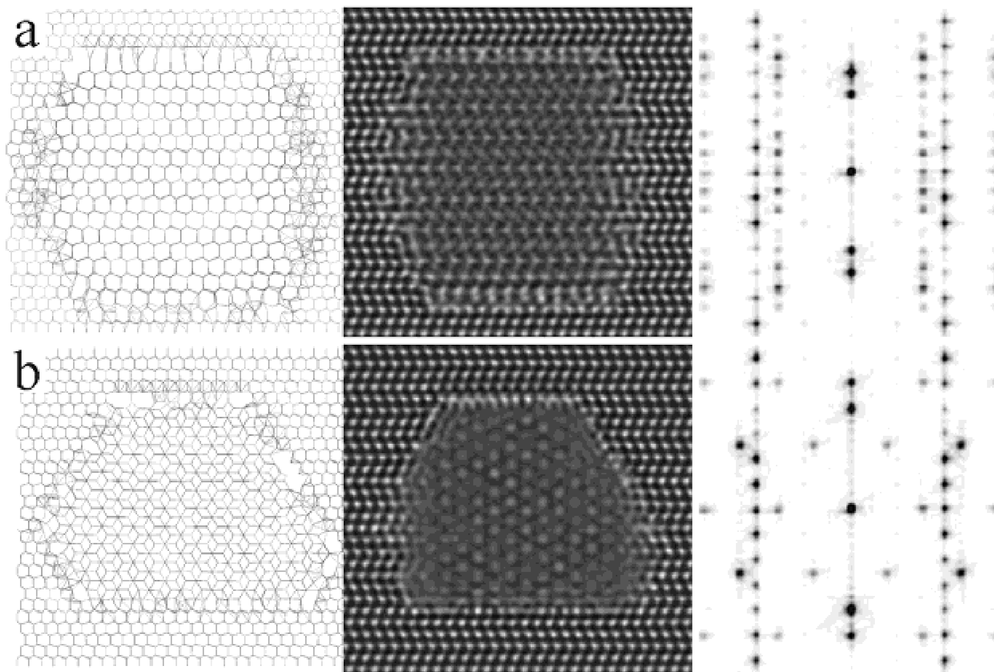

Fig. 7: Nanocrystal within *4H*-SiC oriented in view A (a) and view C (b); on the left: atomic models after MD-relaxation, middle: corresponding simulated HRTEM images, right: FFT patterns.

In view A, stacking faults are directly revealed, as well as in view B. In views C and D, the stacking faults in the nanocrystals are not seen as they lay in the plane parallel (in view C the stacking faults are parallel to $[11\bar{2}0]$ of the matrix) or inclined (view D) to the projected view of the nanocrystal. As the nanocrystals can be revealed only in very thin areas of the specimen, real statistics about their orientations is not possible. As an estimate, from 11 nanocrystals revealed within one area of a TEM specimen, we obtained the following result: 5 view A (3 elongated, 2 compact), 1 view B, 1 view C, 4 view D. In accordance with the general observation during the study of a number of TEM specimens this suggests that for the implantation and annealing conditions studied, nanocrystals in views A and D are most common. In addition, from the viewpoint of their habitus, two main classes of dots are observed: facetted and more spherically shaped. The latter are usually very small (see Fig. 5 b_1, b_1, c_2). Faceting is remarkable revealed only in view C and D. Moreover, from the viewpoint of their aspect ratios (length-to-width) viewed in $[11\bar{2}0]$ matrix projection, two classes are found, elongated and compact dots. We are going to clarify why the four different orientations A, B, C, and D are found for the nanocrystals of different habitus and shape.

Fig. 2 shows a model of the nanocrystal in view A and the corresponding notation of the crystal axes. A rotation of the nanocrystal around its a-axis by $\vartheta = 90°$ transfers it from view

A (Fig. 7a) to view C (Fig. 7b). In the middle and on the right of the figure, the simulated HRTEM images and corresponding diffractograms obtained on the base of the MD-relaxed models (left) are shown. As can be seen there is a qualitative good agreement between the experimental (see in Figs 5 and 6, (a_3) and (c_1)) and the simulated images and diffractograms. (A more detailed comparison between the interface details of simulated HRTEM images based on relaxed and unrelaxed atom coordinates with the experimental image will be reported in due course).

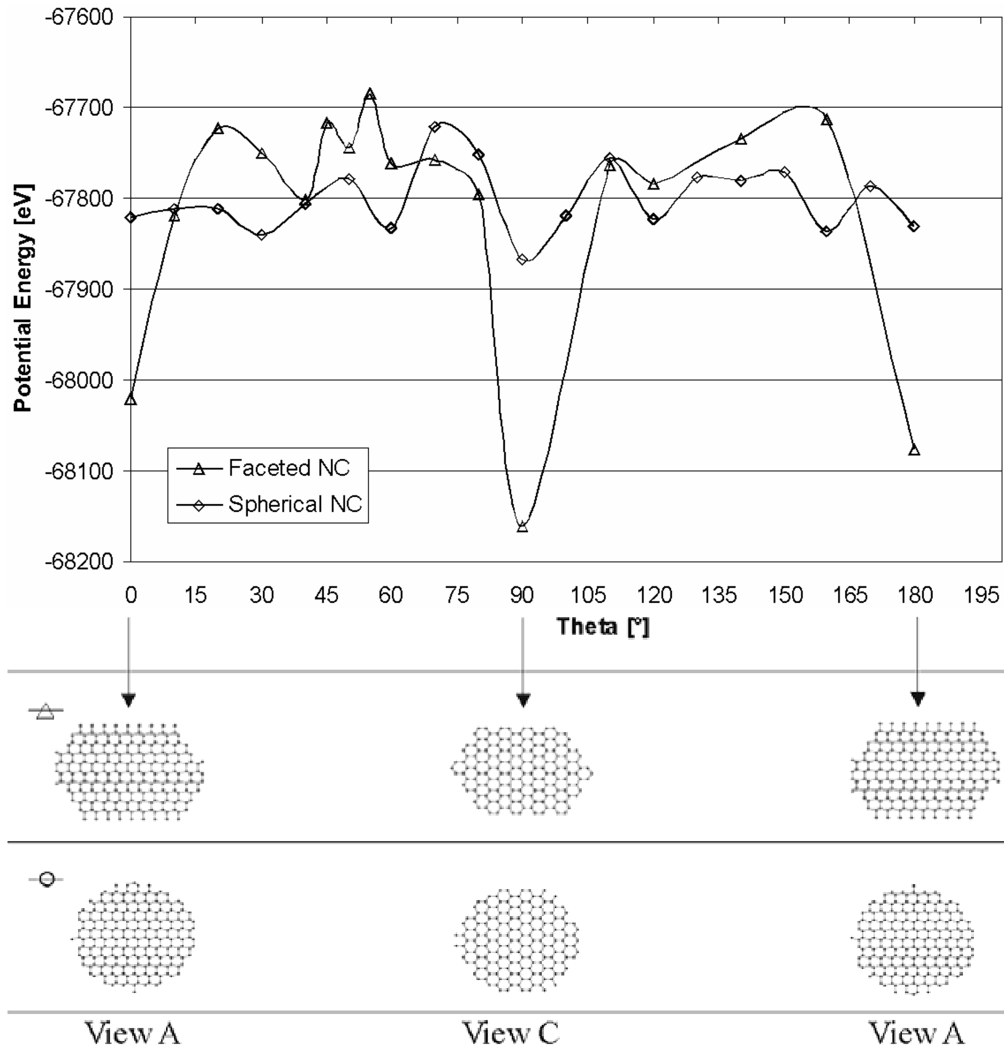

Fig. 8: Potential energy plots of faceted and spherical nanocrystals as a function of the rotation angle ϑ. When rotating the nanocrystals by 180° it is clearly seen that the faceted shaped nanocrystal shows strong energetic minima for view A as well as for view C, however the spherical nanocrystal does not show deep energetic minima. Both nanocrystal models contain the same number of atoms (3000).

The potential energy of the whole structure (nanocrystal and surrounding SiC matrix) as a function of the rotation of a facetted respectively a spherical nanocrystal around the a-axis (see Fig. 2) is shown in Fig. 8. It is clearly seen that the facetted nanocrystal shows strong minima of the potential energy at ϑ equal to 0° or 180° (view A) and at ϑ equal to 90° (view C). A spherical nanocrystal of the same size however does not show pronounced minima. (It has been proved in addition for the spherical nanocrystal model that also rotation around the other axes b and c does not result in pronounced minima). This explains why those nanocrystals could also be found in view B. However, well facetted nanocrystals appear in view A or C in accordance with the strong minima of the potential energy.

To study the influence of the aspect ratio of the length to the width of a nanocrystal on the orientation-relationships, the facetted nanocrystal seen in Fig. 8 (with an aspect ratio of 1:1.1) now has been compared to a pronounced elongated nanocrystal (with an aspect ratio of 1:1.8), keeping the number of atoms constant as well as the faceting in both models. The potential energies of the compact and elongated models are shown in Fig. 9. In contrast to the facetted compact nanocrystals with minima in view A and C (see also Fig. 8), the faceted elongated nanocrystal comprises most strong minima only in view A. Thus, the calculations showed that elongated nanocrystals strongly prefer view A and therefore, the nanocrystals in view C should not be elongated parallel to the $[11\bar{2}0]$ direction of the SiC matrix.

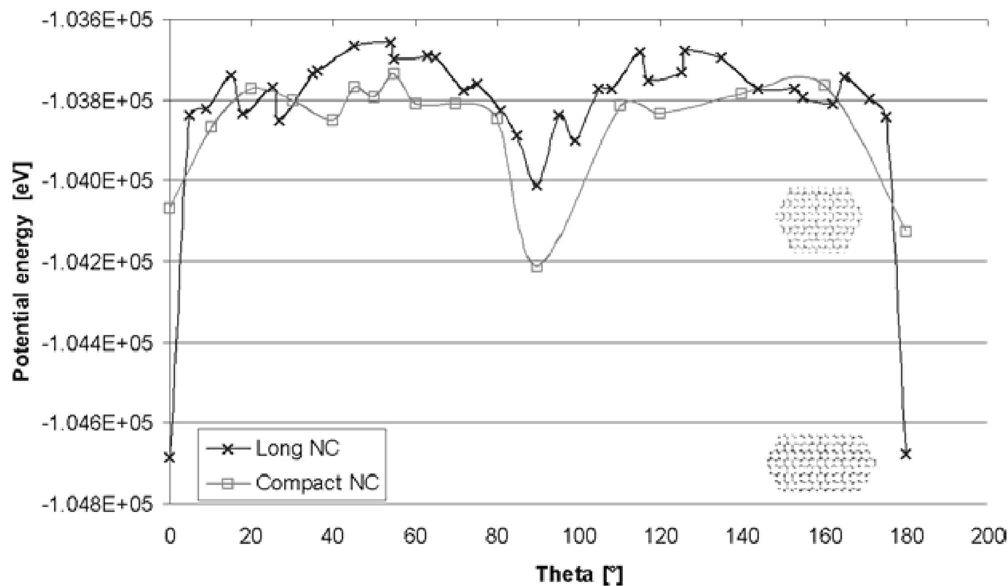

Fig. 9: Potential energy plots of nanocrystals of different aspect ratios (1:1.8 corresponding to an elongated nanocrystal, 1:1.1 corresponding to a compact nanocrystal) but the same number of atoms (4000) as a function of the angle ϑ for rotation from 0 to 180°. The elongated nanocrystal has a strong energetic minimum for view A. The compact nanocrystal shows the strongest minimum in view C. However, in addition a pronounced minimum is seen in view A.

In order to investigate the appearance of nanocrystals in view D projection, the model has been rotated in the following way: Starting from a nanocrystal model projected in view A, it was rotated around the a-axis by ϑ from 85 to 95° and around the c-axis by ψ from 0 to 10°

(see Fig. 2). The potential energy was calculated in steps of 0.5° and resulting HRTEM images have been simulated for selected cases. Two facetted compact nanocrystal models have been investigated, mainly symmetrically and strongly asymmetrically facetted along the c-direction of the *4H*-SiC matrix. Both models contain the same number of atoms. As can be seen, for the first case the 2D plot of the potential energy is almost symmetric around the a-axis (Fig. 10a).

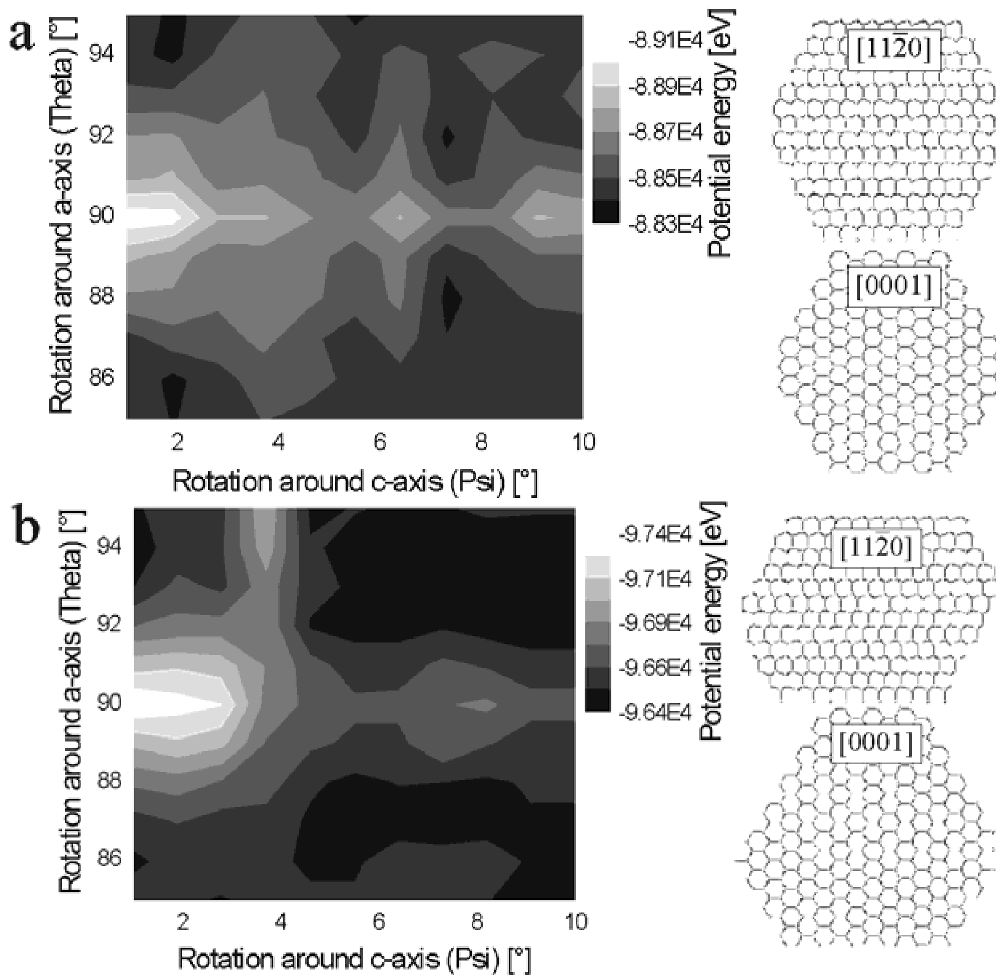

Fig. 10: Potential energy plots as a function of the rotation of the nanocrystal in the fixed *4H*-SiC matrix around ϑ and ψ (see Fig. 6) for two different nanocrystal models with the same number of atoms (3500): (a) symmetrically facetted, (b) asymmetrically facetted showing that in the first case the energy plot is almost symmetric along the c-axis. However, in the second case it is strongly asymmetric. The position of the new strong local minimum corresponds to the view D.

There is a strong minimum at $\vartheta = 90°$, $\psi = 0°$ (view B), and there are two local minima at $\vartheta = 0°$, $\psi = 6.5°$ and at $\vartheta = 90°$, $\psi = 9°$ which however all do not correspond to a nanocrystal of view D as their corresponding HRTEM images show more than the one set of lattice plane

fringes. In contrast, the plot of the potential energy for the asymmetric case shows in addition the appearance of a new local minimum at $\vartheta = 94°$, $\psi = 5.5°$ that is asymmetric along the a-axis (Fig. 10b). The simulated HRTEM image corresponding to these angles is shown in Fig. 11 together with the diffractogram. It clearly demonstrates the appearance of one set of lattice plane fringes. Thus, nanocrystals embedded in hexagonal *4H*-SiC observed in view D are expected to be strongly asymmetrically facetted. In summary, the shape of the nanocrystal has an important influence on its orientation within the matrix. Further, for different orientations it is expected that very different matrix-nanocrystal interface structures and interface strains are created.

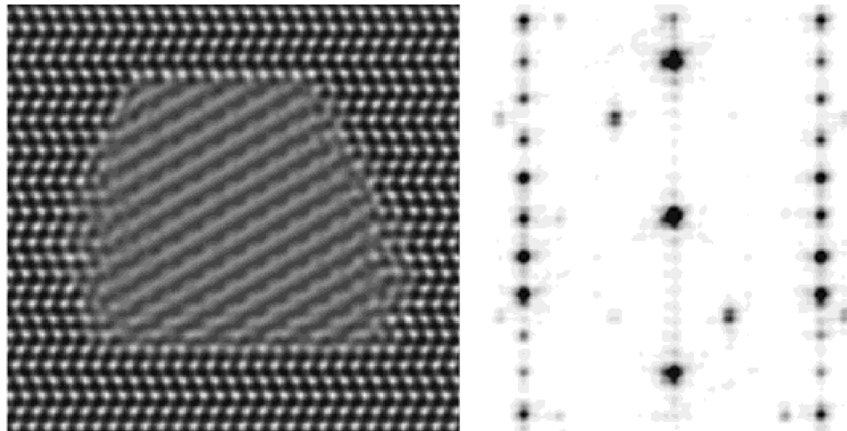

Fig. 11: Simulated $(11\bar{2}0)$ HRTEM image together with their diffractogram showing that a rotation of the nanocrystal within *4H*-SiC (fixed at $(11\bar{2}0)$ orientation) from view C (a) by $\vartheta = 6°$ and $\psi = 4°$ results as shown in (b) in the appearance of only one $\{01\bar{1}0\}$ lattice plane corresponding to view D.

For selected nanocrystals, a Ge content between 70 and 90 % was determined by EDX analysis [KAISER (b)]. In Table 1 the experimental $(01\bar{1}0)$ d- values for the nanocrystals obtained from the g-vector analysis of the diffractograms (see Fig. 5) are summarized. As seen from the comparison to the table value for an averaged content of 80% Ge shown in Table 2, all experimental values are much smaller. Therefore two Si nanocrystals, created after Si implantation into SiC have been analysed, which, interestingly, have a high degree of hexagonality also. Their $01\bar{1}0$-reflection d-spacing was analysed and surprisingly, the nanocrystals show values of 2.8% smaller than the $01\bar{1}0$ Si table value (see Table 2). As a very rough estimate, we apply the same strain value to the GeSi nanocrystals, which then results in a d-value of the $(01\bar{1}0)$ lattice fringe spacing of 0.333 nm (Table 1). As seen, this value is a good average of the measured values, however, it is hard to explain by an elastic compression of the nanocrystals. It may be proposed that the smaller lattice parameters of the GeSi (respectively Si) nanocrystals arises due to a high nonequilibrium concentration of vacancies created during the process of nanocrystal formation at the high annealing temperature and subsequent cooling down, (which very likely goes over the melted state of

the GeSi respectively Si nanocrystals). Further, nanocrystals in view C and D seem to be more strained than those in view A and B. To make more exact conclusions, however, the content of each particular nanocrystal has to be determined separately.

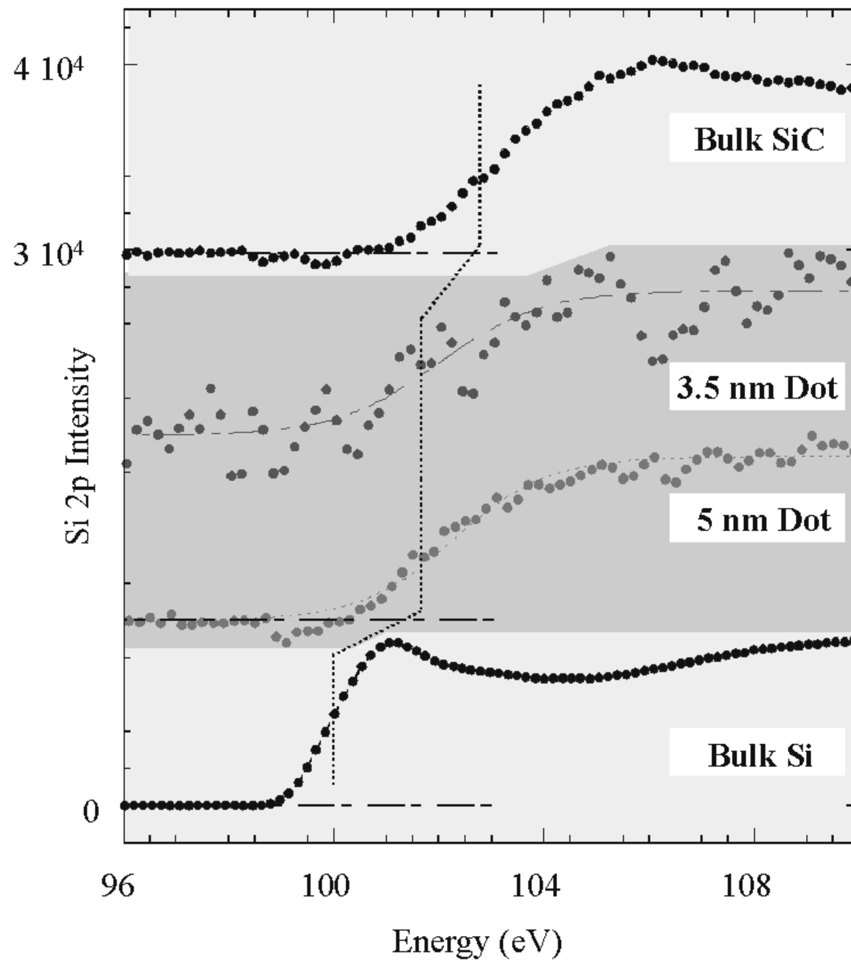

Fig. 12. EELS-spectra showing the intensity around the Si L_3 edge in the *4H*-SiC matrix (upper part) in the GeSi nanocrystals (middle part) and for comparison in pure Si (lower part). The shift of the edge onset for the case of the nanocrystal is clearly seen. For comparison: $SiL_{bulk\ SiC}$: 103 eV, $SiL_{bulk\ Si}$: 99.84 eV. The 5nm dot showed instead 101.8±0.5 eV and the 3.5 nm dot 102.0±0.5 eV.

Table 1: Measured $01\bar{1}0$ d-values from the nanocrystals presented in Fig. 5 (direct space), and Fig. 6 (reciprocal space) obtained from the examination of the $01\bar{1}0$ reflections.

	1	2	3
Fig. 5a	0.338	0.337	0.334
Fig. 5b	0.334	0.335	0.335
Fig. 5c	0.330	0.329	0.331
Fig. 5d	0.330	0.326	0.325

Table 2: Table values for $01\bar{1}0$ lattice planes of cubic Si and Ge in hexagonal projection and for $Ge_{0.8}Si_{0.2}$ calculated in accordance to the Vegard's law, as well as for a 2.8% strained $Ge_{0.8}Si_{0.2}$ nanocrystal.

Element	Si	Ge	$Ge_{0.8}Si_{0.2}$	Strained $Ge_{0.8}Si_{0.2}$ (2.8%)
$d_{01\bar{1}0}$ [nm]	0.332	0.346	0.343	0.333

Two differently sized and oriented nanocrystals (3.5 nm crystal in view B, see Fig. 5b_3 and 5 nm crystal in view D, see Fig. 5d_2) have been analysed by high spatial resolution EELS combined with atomic resolution HAADF imaging. In Fig. 12 the SiL_3 edges measured for the nanocrystals and the SiC matrix together with the spectrum of standard bulk Si are presented, showing pronounced difference in positions and shapes. The SiL_3 edge position for 100% unstrained bulk Si is at 99.85 eV. For both nanocrystals it shifts to higher energies; for the 3.5 nm GeSi nanocrystal to 101.8 ± 0.5 eV, and for the 5nm crystal to 102.0 ± 0.5 eV. Within the error of the measurement, the SiL_3 edge energy for both GeSi nanocrystals studied are identical.

The SiL_3 edge for bulk SiC is shifted to even higher energies, to 103eV. The results can be explained in the following way. As it has been determined from the ADF contrast analysis that both nanocrystals contain about 80±10% Ge, the energy of the SiL_3 edge of 100.3 eV obtained by Morcoc et al. [MORAC] for unstrained thick layers of Si_xGe_{1-x} with 80 % Ge can be used as a standard. It was checked experimentally (by C-K edge EELS) that the GeSi nanocrystals contain no C, therefore the shift of the SiL_3 edge position to higher energy values than 100.3 eV can not be explained by a chemical shift (as it is the case for SiC). However, the shift may be explained by three-dimensional quantum confinement, mainly as an effect of the small size. It should be noted that the SiL_3 edge shape and position of the GeSi nanocrystals is strikingly similar to the 3-4 nm diameter Si nanoclusters within SiO_2, analyzed by Batson et al. [BATSON (b)].

Summary and conclusion

Models of differently shaped hexagonal GeSi nanocrystals embedded in *4H*-SiC have been created and their potential energy has been determined by molecular dynamics calculations as a function of the rotation angles of the nanocrystal within the matrix. It has been found that the four main orientation-relationships experimentally observed in high-resolution TEM images of GeSi nanocrystals correlate with their actual shape and can be explained by strong minima of the potential energy of the nanocrystal-matrix system. For two selected small nanocrystals examined with atomic-resolution annular dark-field scanning TEM and Si L edge energy loss spectra, for the first time, the quantum confinement of the $Ge_{0.8}Si_{0.2}$ nanocrystals buried in *4H*-SiC has been demonstrated and addressed (in accordance to calculations [KATULA]) to the effect of the small size.

However more nanocrystals need to be investigated, and even higher energy resolution experiments performed in order to determine the influence of quantities like strain and composition on the electronic structure. As it has been shown that the nanocrystals differ strongly in their sizes, measurements of the electronic properties averaging over the whole host crystal volume may not be helpful and moreover matrix damage may obscure the properties of the individual nanocrystals. However, by varying the implantation and

annealing parameters it may be possible to control the dimensionality and matrix defect state, and the hence electronic properties, of the resultant nanocrystals.

Acknowledgements

The authors are grateful to Andrey Chuvilin for help in the field of high-resolution image simulations and to Larissa Starovoitowa for TEM sample preparation. We acknowledge the financial support of this research by the Deutsche Forschungsgemeinschaft Sonderforschungsbereich 196.

References

BATSON (a), P. E. : Nature 366 (1993) 727-728
BATSON (b), P. E., HEATH, J. R.: Phys. Rev. Lett. 71 (1993) 911-14
BENABBAS, T., ANDROUSSI, A, LEFEBVRE, A.: J. Appl. Phys. 86 (1999) 1945
BORDING, J. K. , TAFTE, J.: Phys. Rev. B 62 (2000) 8098
BROWNING, N. D. , CHISHOLM, M. M., PENNYCOOK, S. J.: Nature 366 (1993) 143-146
CHRISTIANSEN, S., ALBRECHT, M., STRUNK, H. P., MAIER, H. J.: Appl. Phys. Letter 64 (1994) 3617
CHUVILIN, A., CHESNOKOVA, T. E.: XVI RKEM, Chernogolovka (1996) 34
COLOMBO L, RESTA R., BARONI, S.: Phys. Rev. B 44 (1991) 5572
COMBE, N., JENSEN, P., PIMPINELLI, A.: Phys. Rev. Lett. 85 (2000) 110
COWLEY, J. M. AND MOODIE, A. F.: Acta Cryst. 10 (1957) 609-619
CREWE, A. V. , WALL J., LANGMORE, J. P.: Science 168 (1970) 1338
CROZIER, P. A,TSEN, S. C. Y., LIU, J., LOPEZ, C. & CARZEZ, J. A.,: Journal of Electron Microscopy 48 (1999) 1015-1024
DAHMEN, U., XIAO, S. Q., PACIORNIK, S., JOHNSON, E, JOHANSEN. A.: Phys. Rev. Let. 78-3 (1997) 471-474
DE RUIJTER W.J. , SHARMA, R., MCCARTNEY, M. R., SMITH, D. J.: Ultramicrosopy 57 (1995) 409-422
GÄRTNER, K., & WEBER, B.: Nuclear Instruments and Methods B 180 (2001) 274
HOWIE, A.: J. Microscopy 17 (1979) 11-23
KAISER (a), U., CHUVILIN, A.: submitted Microsc. & Microanal.
KAISER (b), U.: J. Electron. Micros. 50 (2001) 251
KATULA, G., GUEDI C., KOLODZY, J., WILSON, R. G. , SWAN, C., TSAO, M. W., RABOLT, J.: Appl. Phys. Let. 74-4 (1999) 540
KOHN, W., SHAM, L. J.: Phys. Rev. 140 (1965) A1133-A1138
LANÇON, F., PENISSON, J.-M., DAHMEN, U.: Europhysics Lett. 49 (2000) 603
LOANE, R. F. ,KIRKLAND, E. J., SILCOX, J.: Acta. Cryst. A 44 (1988) 912-927
MORAC, J. P., BATSON, P. E., TERSOFF, J.: Phys. Rev. B. 47 (1993) 4107-4110
MORIGUCHI, K. & SHINTANI, A.: Jpn. J. Appl. Phys. 37(1998) 414
MULLER (a), D. A. , SORSCH, T., MOCCIO, S., BAUMANN, F., EVANS-LUTTERODT, K., & TIMP, G.: Nature 399 (1999) 758-761
MULLER (a), D. A. , TZOU, Y. ,RAJ, R., SILCOX, J.: Nature 366 (1993) 725 - 727
NIQUET, Y. M., ALLEN, G., DELERUE, C. ,LANNOO, M.: Appl. Phys. Let. 77 (2000) 1182
O'KEEFE, M. A. , KILAAS, R.: Scanning Microscopy Supplement 2 (1988) 225
PANDEY, R., RÉRAT, M., DARRIGAN, C., CAUSÀ, M.: Jour. of Appl. Phys. 88 (2000) 6462
PAUWELS (a), B., VAN TENDELOO, G., BOUWEN, W., THEIL KHUN, L., LIEVENS, P., LEI, H., HOU, M.: Phys. Rev. B 62 (2000) 10282
PAUWELS, (b), B., VAN TENDELOO, G., ZHURKIN, E., HOU, M. VERSCHOREN, G., THEIL, L., BOUVEN, W., LIEVENS, P.: Phys. Rev. B 63 (2001) 165406
PENNYCOOK, S. J. Z.: Ultramicroscopy 30 (1989) 58-69
PERESSI (a), M., COLOMBO L., RESTA, R., BARONI, S.: Phys. Rev. B 48 (1993) 12047
PERESSI (b), M., BARONI, S. , BALDERESCHI, A., RESTA, R.: Phys. Rev. B 41 (1990) 12106
SCHEERSCHMIDT, K., CONRAD, D., KIRMSE, H., SCHNEIDER, R., NEUMANN; W.: Ultramicroscopy 81 (1999) 289-300

SCHUBERT, CH., KAISER, U., GORELIK, T., HEDLER, A., KRÄUßLICH, J., WUNDERLICH, B., HEß, G., GOETZ, K., GLATZEL, U., WESCH, W.: J. Appl. Phys. 91 (2002) 1520
STILLINGER, F. H. , WEBER, T. A.: PHYS. REV. B 31 (1985) 5262
TAKEOKA, S.: Phys. Rev. B 58 (1998) 7921
TERSOFF (a), J.: Phys. Rev. B 37 (1988) 6991-6700
TERSOFF (b), J.: Phys. Rev. B 38 (1988) 5002-5005
TERSOFF (c), J.: Phys. Rev. B 39 (1989) 5566-5568
TERSOFF (d), J.: Phys. Rev. Let. 61 (1988) 2879
THON, F., WILLASCH, D.: Optik 36 (1972) 55-58
VERLET, L.: Phys. Rev. 159 (1967) 98
WEISSKER, H.-C., FURTHMÜLLER, J., BECHSTEDT, F.: Physica status solidi B 224 (2001) 769-773
WERNER, P., SCHEERSCHMIDT, K., ZAKHAROV, N. D., HILLEBRAND, R., GRUNDMANN, M., SCHNEIDER, R.: Cryst. Res. Technol. 35 (2000) 759-768
ZIMMERMANN, C. G. , NORDLUND, K., GIBSON, J. M., AVERBECK, R. S., HERR, U., SAMWER, K.: Phys. Rev B 64 (2001) 085419